RSC Advances

This is an *Accepted Manuscript*, which has been through the Royal Society of Chemistry peer review process and has been accepted for publication.

Accepted Manuscripts are published online shortly after acceptance, before technical editing, formatting and proof reading. Using this free service, authors can make their results available to the community, in citable form, before we publish the edited article. This *Accepted Manuscript* will be replaced by the edited, formatted and paginated article as soon as this is available.

You can find more information about *Accepted Manuscripts* in the Information for Authors.

Please note that technical editing may introduce minor changes to the text and/or graphics, which may alter content. The journal's standard Terms & Conditions and the Ethical guidelines still apply. In no event shall the Royal Society of Chemistry be held responsible for any errors or omissions in this *Accepted Manuscript* or any consequences arising from the use of any information it contains.

ROYAL SOCIETY OF CHEMISTRY

www.rsc.org/advances

Ultrafine PEG-capped gadolinia nanoparticles: cytotoxicity and potential biomedical applications for MRI and luminescent imaging

Timur Sh. Atabaev[1*], Jong Ho Lee[2], Dong-Wook Han[2*], Hyung-Kook Kim[3*] and Yoon-Hwae Hwang[3*]

[1] *Department of Nano Materials Engineering, College of Nanoscience and Nanotechnology Pusan National University, Miryang 627-706, Republic of Korea*

[2] *Department of Applied Nanoscience, College of Nanoscience and Nanotechnology, Pusan National University, Busan 609-735, Republic of Korea*

Corresponding authors: atabaev@snu.ac.kr, nanohan@pusan.ac.kr, hkkim@pusan.ac.kr and yhwang@pusan.ac.kr

Abstract

In recent years, magnetic and luminescent nanoparticles (NPs) have attracted considerable attention recently because of their potential applications in nanomedicine. In this study, bimodal ultrafine polyethylene glycol (PEG) -capped gadolinium oxide NPs doped with erbium ions, which combine both paramagnetic and luminescent properties in a single entity, were synthesized using the urea homogeneous precipitation route. The morphological, chemical and structural properties of the synthesized particles were examined using a range of microscopy and energy-dispersive X-ray techniques. The optical characteristics of the gadolinium oxide NPs were examined by analyzing the room temperature emission spectra, which correspond to various manifold transitions of Er^{3+}. Pilot studies were performed to examine the cytotoxicity and capability of the synthesized NPs for the luminescent labeling of living C2C12 myoblastic cells. The paramagnetic properties of the synthesized particles as a magnetic resonance imaging MRI contrast agent were also assessed. Overall, these synthesized ultrafine PEG – coated Gd_2O_3:Er^{3+} NPs can potentially be used in biomedical applications because of their strong positive contrast enhancement in T_1-weighted imaging, and intense green emission with near-infrared (NIR, 980 nm) excitation.

Keywords: Gadolinia, nanoparticles, cytotoxicity, MRI contrast agent

1. Introduction

Luminescent NPs are some of the most promising tools for sensing, manipulation and detection of biological systems. In particular, lanthanide (Ln^{3+})-based inorganic NPs are an emerging class of advanced nanomaterials that can be used successfully in a range of biomedical applications, such as

RSC Advances Accepted Manuscript

optical imaging and contrast agents for magnetic resonance imaging (MRI), therapeutics.[1, 2] Furthermore, Ln^{3+}-doped luminescent nanoparticles are quite photostable, exhibiting long luminescence lifetimes and narrow emission bands compared to quantum dots (QDs). The optical properties arise from the many possible electronic transitions between the metastable states of Ln^{3+}-doped ions. Among them, the erbium ion (Er^{3+}) is an excellent dopant candidate because the intermediate $^4I_{9/2}$ and $^4I_{11/2}$ (~ 800 and 980 nm) levels are easily excitable with near-infrared (NIR) radiation. The use of NIR excitable nanoparticles, which are less toxic than UV excitable QDs, can increase the penetration depth and suppress autofluorescence in biological samples. In addition, partially filled 4-*f* orbitals are also responsible for the magnetic properties of Ln^{3+}-doped luminescent nanoparticles. For example, the 7 unpaired electrons in Gd^{3+} are the prime reason for why this ion is used in MRI because it changes the spin–lattice relaxation of the protons of the coordinated and nearby water; hence it is a T_1 contrast agent. Gd^{3+} brightens the imaging where it is present, making it a positive contrast agent, unlike SPIONs (superparamagnetic iron oxide nanoparticles), which affect the spin–spin relaxation and darken the image, making it a negative T_2 contrast agent. [3, 4]

Typical imaging methods, such as fluorescence imaging and magnetic resonance imaging, have different sensitivities, spatial resolutions, and imaging depths. [5] In vivo fluorescence imaging provides high sensitivity and temporal resolution but the penetration of visible light in living tissues is inefficient and the spatial resolution is limited. MRI can produce non-invasive images with functional information and high spatial resolution anatomic details based on the soft-tissue contrast. Therefore, a range of multimodal imaging probes, combining different imaging modalities are particularly interesting because they have unusual properties needed for more accurate imaging and diagnosis. For example, nanoparticles combining a fluorescence imaging modality and MRI modality offer the advantages of fluorescence imaging, i.e., high sensitivity, along with the high spatial resolution anatomic imaging capability of MRI. Up to now, magnetic nanoparticles based on iron oxides (Fe_2O_3 or Fe_3O_4) are the only ones permitted for use in the *in-vivo* examinations of patients, but there has been some interest in developing novel, more efficient systems, e.g., nanoparticles contrast agent-based highly magnetic rare earth metals. Gd_2O_3 NPs and mixed rare-earth/transition metal oxides are promising candidates for use in MRI. The Gd_2O_3 NP-based system is expected to yield a considerably higher relaxivity due to the higher density of magnetic ions. Other benefits would be the less leakage of Gd^{3+} ions and the greater opportunities for surface modification and possible targeting properties. Furthermore, considerable efforts have been made to minimize the toxicity of Gd_2O_3-based NPs.

In this study, ultrafine bimodal Er^{3+}-doped Gd_2O_3 NPs (Gd_2O_3:Er^{3+} NPs) were fabricated using a facile urea homogeneous precipitation method. The morphology, structural, chemical and magnetic properties

RSC Advances Accepted Manuscript

of the prepared $Gd_2O_3:Er^{3+}$ NPs were examined using a range of microscopy and analysis techniques. The optical characteristics were examined by analyzing the room-temperature emission spectra, which correspond to various manifold transitions of Er^{3+}. In the second step, the surface of the $Gd_2O_3:Er^{3+}$ NPs was coated with a thin layer of biocompatible PEG to achieve higher biocompatibility and enhance steric repulsion between the synthesized NPs. The cytotoxicity and capability of the PEG-coated $Gd_2O_3:Er^{3+}$ NPs for the luminescent labeling of living cells were also performed using a C2C12 myoblastic cell line.

2. Experimental details

2.1 Synthesis of PEG-coated $Gd_2O_3:Er^{3+}$ NPs

Analytical grade Gd_2O_3 (99.9 %), Er_2O_3 (99.9 %), HNO_3 (70 %), polyethylene glycol (PEG, average M_n 4000) and urea (99.0-100.5%) were purchased from Sigma-Aldrich and used as received. Spherical $Gd_2O_3:Er^{3+}$ NPs were fabricated using a urea homogeneous precipitation method using the reported protocols. [6-8] First, a sealed beaker with a freshly prepared aqueous solution of rare-earth nitrates (0.001 mol in 40 ml of H_2O) was placed into an electrical furnace and heated to 90 °C for 1.5 h. The doping concentration of Er^{3+} was kept to 1 mol.%. The dried synthesized precipitates were then calcined in air at 800 °C for 1 h to produce the oxide NPs. Second, a sealed beaker containing the dispersed $Gd_2O_3:Er^{3+}$ NPs (2 mg) and an aqueous solution of PEG (5g in 50 ml of H_2O) was heated to 150 °C for 2 h. The NP suspension was then cooled to room temperature, followed by dialysis in deionized ultrapure water for 24 h, to eliminate the free Gd^{3+} ions and PEG excess. The PEG-coated $Gd_2O_3:Er^{3+}$ NPs were isolated by centrifugation and dried at room temperature for 1 day.

2.2 Physical characterization

The structure of the prepared powders was examined by XRD (Bruker D8 Discover) using Cu-Kα radiation (λ = 0.15405 nm) at a 2θ scan range 20–60° 2θ. The morphology of the particles was characterized by field emission transmission electron microscopy (FETEM, JEOL JEM-2100F). Elemental analysis was carried out using energy dispersive X-ray spectroscopy (EDX, Horiba, 6853-H). The structural properties of the prepared samples were analyzed by Fourier transform infrared (FTIR, Jasco FT/IR6300) spectroscopy. The down-conversion photoluminescence PL measurements were performed using a Hitachi F-7000 spectrophotometer equipped with a 150 W Xenon lamp as the excitation source. In addition, to record the up-conversion emission spectra of the PEG-coated $Gd_2O_3:Er^{3+}$ NPs, a commercially available 980 nm diode laser was used as the excitation source. The magnetization measurements were performed by quantum design vibrating sample magnetometry (QD-VSM, physical properties measurement system PPMS 6000). The T_1-weighted images were obtained using a 1.5 T MRI

RSC Advances Accepted Manuscript

scanner (General Electric, Signa, HDx1.5T, USA) using the T_1-weighted spin-echo method [TR/TE = 500 ms/15 ms, field of view (FOV) = 180 mm × 180 mm, slice thickness = 2 mm, matrix = 256 × 204, number of excitations (NEX) = 2]. All measurements were performed at a room temperature of 22 ± 1 °C.

2.3 Cell culture and cytotoxicity assay

A murine myoblast cell line (C2C12 cells derived from the thigh muscle of C3H mice) was obtained from the American Type Culture Collection (ATCC CRL-1172™, Rockville, MD). Cells were routinely maintained in Dulbecco's modified Eagle's medium (DMEM, Sigma-Aldrich Co., St Louis, MO), supplemented with 10 % fetal bovine serum (Sigma-Aldrich Co.) and 1% antibiotic antimycotic solution (including 10,000 units penicillin, 10 mg streptomycin and 25 μg amphotericin B per ml, Sigma-Aldrich Co.) at 37°C in a humidified atmosphere containing 5% CO_2. The number of viable cells was indirectly quantified by using a cell counting kit-8 (CCK-8, Dojindo, Kumamoto, Japan), which contains highly water-soluble tetrazolium salt [WST-8, 2-(2-methoxy-4-nitrophenyl)-3-(4-nitrophenyl)-5-(2,4-disulfophenyl)-2*H*-tetrazolium, monosodium salt] reduced to a yellow-color formazan dye by mitochondrial dehydrogenases. The cell viability was found to be directly proportional to the metabolic reaction products obtained in this assay. Briefly, the CCK-8 assay was conducted as follows. The suspension of C2C12 cells was seeded at a density of 1×10^5 cells mL^{-1} in a 96-well plate and was then cultured in a complete DMEM at 37°C under 5% CO_2 until grown as monolayer cultures. Cultured cells were treated with increasing concentrations (0 ~ 250 ppm) of PEG-coated Gd_2O_3:1% Er^{3+} NPs and were then incubated with WST-8 solution for the last 4 h of the culture period (24 h) at 37°C in the dark. Since residual NPs can affect the absorbance values at 450 nm, the cells exposed to NPs were thoroughly washed with 1 × Dulbecco's phosphate-buffered saline (DPBS, pH = 7.0 ~ 7.4, Sigma-Aldrich Co.) prior to incubation with WST-8 solution. Parallel sets of wells containing freshly cultured nontreated cells were regarded as negative (–) controls. The absorbance was determined at 450 nm using an ELISA reader (SpectraMax® 340, Molecular Device Co., Sunnyvale, CA). The relative cell viability was determined as the percentage ratio of the optical density in the medium (containing NPs at each concentration) to that in the fresh control medium. The IC_{50}, the concentration (%) inhibiting the growth of cells by 50%, was estimated from the relative cell viability profiles.

2.4 Fluorescence microscopy

C2C12 cells were seeded at a density of 5×10^5 cells mL^{-1} in a 24-well plate and were then cultured for the qualitative study of the cellular uptake, distribution and subsequent cell imaging

RSC Advances Accepted Manuscript

of PEG-coated Gd_2O_3:1% Er^{3+} NPs. After grown as monolayer cultures with about 80% confluence, adherent cells were washed twice with 1 × DPBS. NP suspension in the media at 10 ppm was then added to the well. Following incubation for 2 h, cells were washed three times with 1 × DPBS and then fixed with 3.5% paraformaldehyde (Sigma-Aldrich Co.) in 0.1 M phosphate buffer (pH 7) for 5 min at room temperature, which was further washed twice with 1 × DPBS. The nuclei were counterstained with 10 μmol/L 4',6-diamidino-2-phenylindole (DAPI, Sigma-Aldrich) immediately before 20 min of observation. The cell monolayer was washed twice with 1 × DPBS and imaged with a fluorescence microscope (IX81-F72, Olympus Optical Co, Osaka, Japan).

2.5 Statistical analysis

All variables were tested in three independent cultures for cytotoxicity assay, which was repeated twice (n = 6). Quantitative data are expressed as the mean ± standard deviation (SD). Data were tested for homogeneity of variances using the test of Levene, prior to statistical analysis. Multiple comparisons to detect the dose-dependent effects of PEG-coated Gd_2O_3:1% Er^{3+} NPs on C2C12 cells were carried out using one-way analysis of variance (ANOVA, SAS Institute, Cary, NC), which was followed by the Bonferroni test when variances were homogeneous and the Tamhane test when variances were not. The value of $P < 0.05$ was considered statistically significant.

3. Results and discussion

3.1 Fabrication and characterization of PEG-coated Gd_2O_3:Er^{3+} NPs

A facile urea homogeneous precipitation method was used in the typical synthesis of ultrafine Gd_2O_3:1 %Er^{3+} NPs. This method allows the easy synthesis of large quantities of homogeneous rare-earth-doped phosphor NPs with a narrow size distribution and excellent optical properties. The phase purity and crystallinity are two most important parameters that significantly affect the properties of phosphor nanomaterials. Figure 1 shows the XRD pattern of Gd_2O_3:1 %Er^{3+} NPs calcined at 800 °C in air. All XRD peaks can be assigned easily to the standard cubic Gd_2O_3 structure (JCPDS No. 88-2165), which belongs to the *Ia3* (206) space group with a lattice constant a = 1.079 nm. [9, 10] No additional peaks from the doped Er^{3+} could be detected due to the relatively low concentration of dopant ions indicating the

RSC Advances Accepted Manuscript

formation of a pure cubic Gd_2O_3 phase. EDX analysis of Gd_2O_3:1 %Er^{3+} NPs confirmed the presence of erbium ions in the Gd_2O_3 host material, as shown in Figure 1 (Inset).

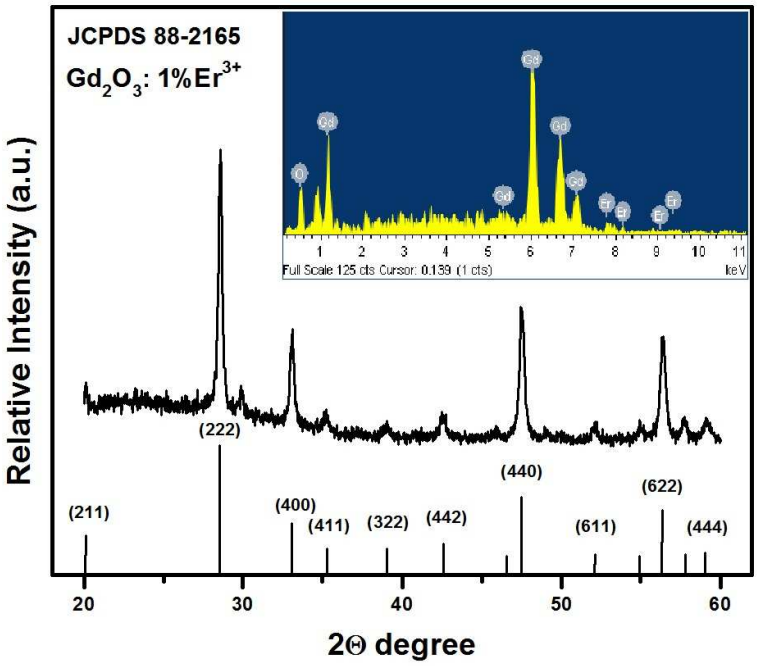

Fig.1 Typical X-ray diffraction pattern of Gd_2O_3:Er^{3+} NPs. Inset shows the EDX analysis data of Gd_2O_3:Er^{3+} NPs.

FETEM was used to characterize the morphology and structure of the PEG-coated Gd_2O_3:Er^{3+} NPs. Figure 2**a** (scale bar – 50 nm) and **b** (scale bar – 10 nm) shows low and high magnification FETEM images of synthesized PEG-coated Gd_2O_3:Er^{3+} NPs, respectively. The sample consisted of well-dispersed NPs with a smooth surface and a narrow size distribution in the range, 88 ± 9 nm. Figure 2**b** also shows that the surface of the NPs was coated with a thin PEG layer (around 2-3 nm). The high resolution FETEM image (Figure 1**c** (scale bar – 2 nm)) revealed continuous lattice fringes, indicating the high crystallinity of Gd_2O_3:Er^{3+} NPs. High crystallinity is very important for phosphors because high crystallinity means fewer traps and stronger luminescence emission. [11] The measured lattice spacing was 0.307 nm, which is close to the reported literature value of d = 0.311 nm for the (222) lattice plane of a pure cubic Gd_2O_3 phase (Figure 1**c**). [9] The selected area diffraction (SAED) pattern taken from the edge of the NPs revealed clear concentric rings from the inside to outside, suggesting the highly crystalline nature of the synthesized Gd_2O_3:Er^{3+} NPs (Figure 1**d**).

RSC Advances Accepted Manuscript

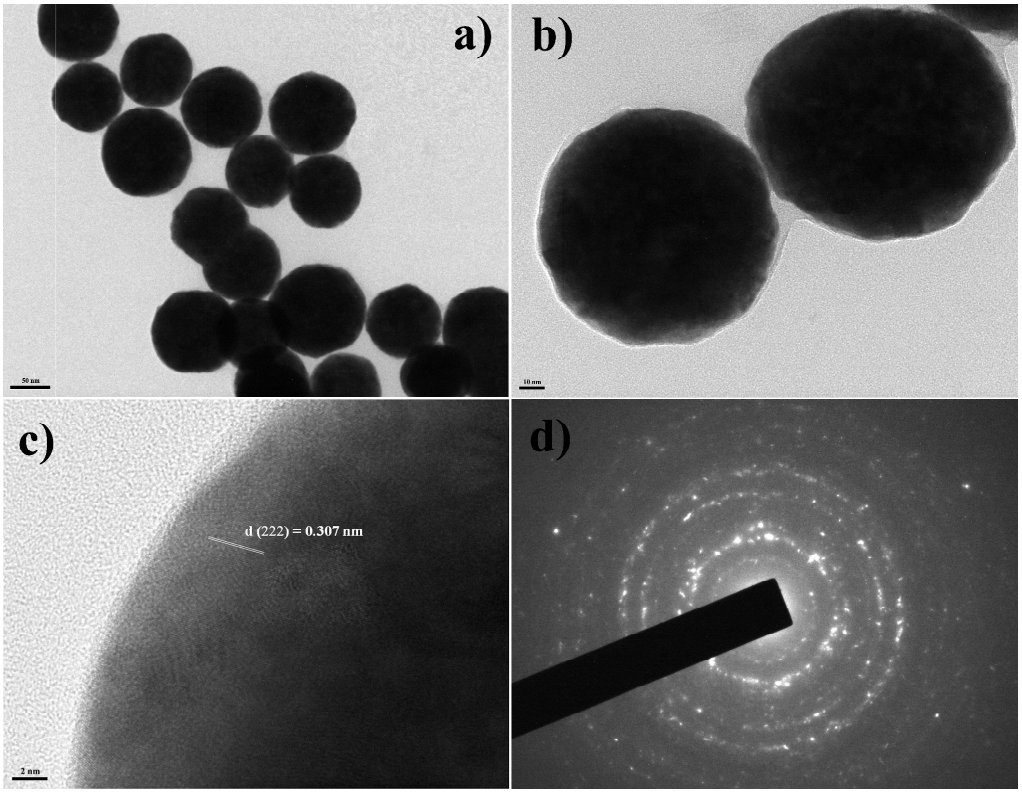

Fig.2 Low (a) and high (b, c) magnification FETEM images of PEG - $Gd_2O_3:Er^{3+}$ NPs. Representative SAED (d) image exhibit highly crystalline nature of the NPs.

The grafting of PEG molecules to the surface of $Gd_2O_3:Er^{3+}$ NPs is highly desirable for prolonging their blood circulation time.[12] Infrared spectroscopy was used to examine the PEG surface-functionalization of the $Gd_2O_3:Er^{3+}$ NPs. The FTIR spectra of the bare $Gd_2O_3:Er^{3+}$ NPs were compared with the spectra for dried PEG-coated $Gd_2O_3:Er^{3+}$ NPs to confirm the successful PEG surface-functionalization. Figure 3 shows the normalized FTIR of the pure $Gd_2O_3:Er^{3+}$ and PEG-coated $Gd_2O_3:Er^{3+}$ NPs. Both samples exhibited the characteristic absorption peaks of metal-oxide Gd-O (~540 cm^{-1}) stretching vibrations of cubic Gd_2O_3.[9] Moreover, both samples exhibited the weak angular deformation of water molecules (~ 1660 cm^{-1}) and the stretch vibrations of the OH group (~ 3600 cm^{-1}). [6] PEG surface-functionalization of the $Gd_2O_3:Er^{3+}$ NPs gives rise to numerous peaks, which were assigned to the different vibrational modes of CH_2. The characteristic peaks arising from scissoring and waging CH_2 vibrational modes were found at approximately 1470 and 1340 cm^{-1}, respectively. [13] Furthermore, the most prominent peak in the spectrum, at approximately 1100 cm^{-1}, was assigned to the PEG chain C-O-C vibrations. [13] Therefore, FTIR further confirmed the formation of a thin PEG coating on the surface of the $Gd_2O_3:Er^{3+}$ NPs.

RSC Advances Accepted Manuscript

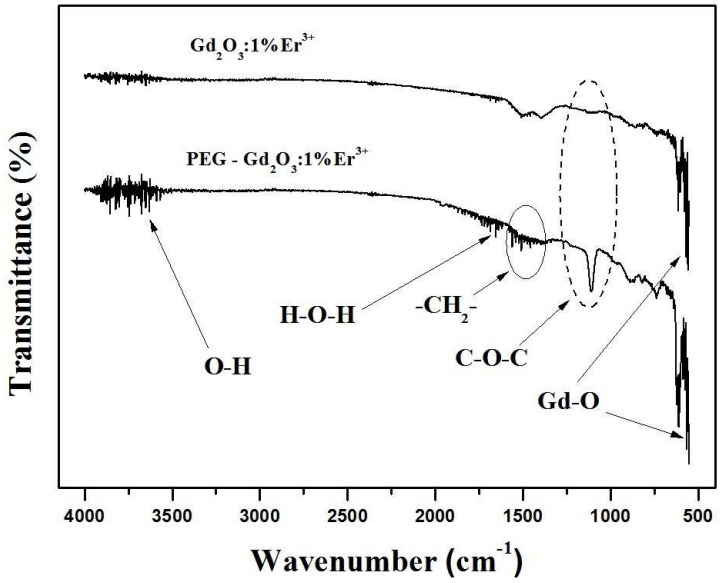

Fig.3 Normalized FTIR spectra of pure $Gd_2O_3:Er^{3+}$ and PEG-coated $Gd_2O_3:Er^{3+}$ NPs

3.2 Optical properties

The luminescent properties of pure $Gd_2O_3:Er^{3+}$ and PEG-coated $Gd_2O_3:Er^{3+}$ NPs were investigated further. Erbium ions have two levels in the NIR spectrum ($^4I_{9/2}$ and $^4I_{11/2}$), ~ 800 and 980 nm, which can be populated conveniently by commercially available low-cost near-infrared NIR laser diodes. Therefore, this study examined their up-conversion UC properties, i.e., their ability to emit light at higher energies compared to the excitation wavelength. Figure 4 shows the normalized up-conversion PL spectra in the range, 450-750 nm, for pure $Gd_2O_3:Er^{3+}$ and PEG-coated $Gd_2O_3:Er^{3+}$ NPs under 980 nm laser excitation. Upon NIR excitation at 980 nm, the emission spectrum showed several main groups of emission lines, which were assigned to the $^4F_{7/2}\rightarrow{}^4I_{15/2}$ (476-494 nm), $^2H_{11/2}\rightarrow{}^4I_{15/2}$ (520-541 nm), $^4S_{3/2}\rightarrow{}^4I_{15/2}$ (545-564 nm) and $^4F_{9/2}\rightarrow{}^4I_{15/2}$ (646-686 nm) transitions within Er^{3+}.[14, 15] A comparison of the PL spectra of the samples showed that the PEG grafting on the surface of $Gd_2O_3:Er^{3+}$ NPs decreases the emission intensity. This was attributed to the luminescence quenching effect of the PEG hydroxyl groups (luminescence killers). [16] The inset in Figure 4 shows the excitation power dependence of the most intense green ($^4S_{3/2}\rightarrow{}^4I_{15/2}$) and red ($^4F_{9/2}\rightarrow{}^4I_{15/2}$) emission signals of the PEG-coated $Gd_2O_3:Er^{3+}$ NPs. Data fitting yielded straight lines with a slope of 1.74±0.07 and 1.68±0.09 for green and red emission, respectively. Therefore, the UC process in the Gd_2O_3:1% Er^{3+} NPs occurs via a two-photon process.

RSC Advances Accepted Manuscript

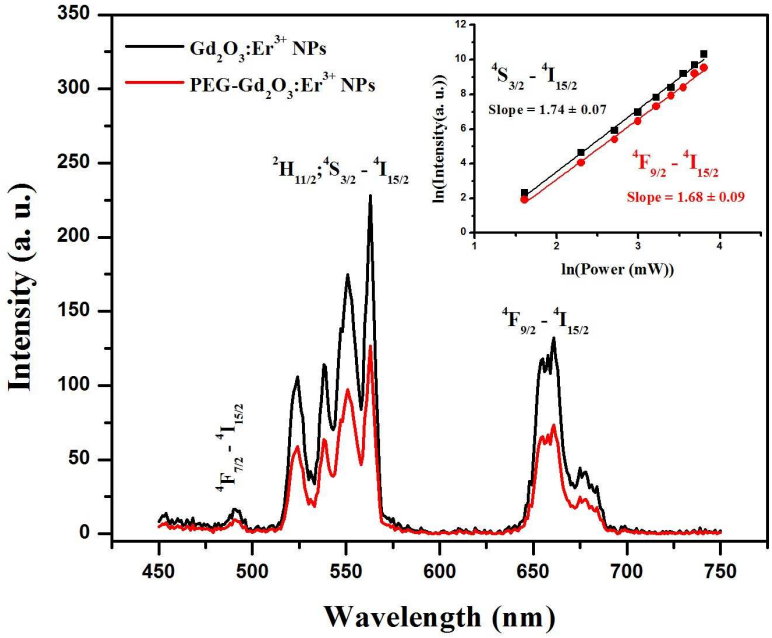

Fig.4 Normalized upconversion emission spectra of pure $Gd_2O_3:Er^{3+}$ and PEG-coated $Gd_2O_3:Er^{3+}$ NPs. Inset shows the excitation power dependent green and red emission signals of PEG-coated $Gd_2O_3:Er^{3+}$ NPs

3.3 Magnetic and relaxivity measurements

To demonstrate the dual-modal capability of the PEG-coated $Gd_2O_3:Er^{3+}$ NPs, T_1-weighted MR images of the UCNP solutions with different NPs concentrations were obtained using a 1.5 T clinical MRI scanner. Because a PEG polymer coating of $Gd_2O_3:Er^{3+}$ NPs is expected to strongly affect the relaxation properties, the MR data for the PEG-capped $Gd_2O_3:Er^{3+}$ NPs were obtained. Figure 5 shows the magnetization vs. applied magnetic field curves *M(H)* taken at room temperature for the PEG-capped $Gd_2O_3:Er^{3+}$ NPs. The *M(H)* curves of the PEG-capped $Gd_2O_3:Er^{3+}$ NPs clearly show typical paramagnetic behavior (linear relationship between magnetization *M* and applied field *H* with a positive slope). Furthermore, as the concentration of the PEG-capped $Gd_2O_3:Er^{3+}$ NPs increased, the T_1-relaxation time of the water protons was shortened significantly, and the T_1-weighted images became brighter, as shown at the top of Figure 5. The slope of the linear fitting of $1/T_1$ vs. Gd^{3+} concentration (Figure 5, inset) yielded a longitudinal relaxivity ($\mathbf{r_1}$) value of 17.69±0.03 mM^{-1} s^{-1}, which is much higher than that of commercial clinical MRI contrast agents, such as Gd-DOTA, Gd-DTPA, Gd-BOPTA, etc. [17] These results suggest that the PEG-capped $Gd_2O_3:Er^{3+}$ NPs can be applied as an effective T_1 contrast agent for MRI.

RSC Advances Accepted Manuscript

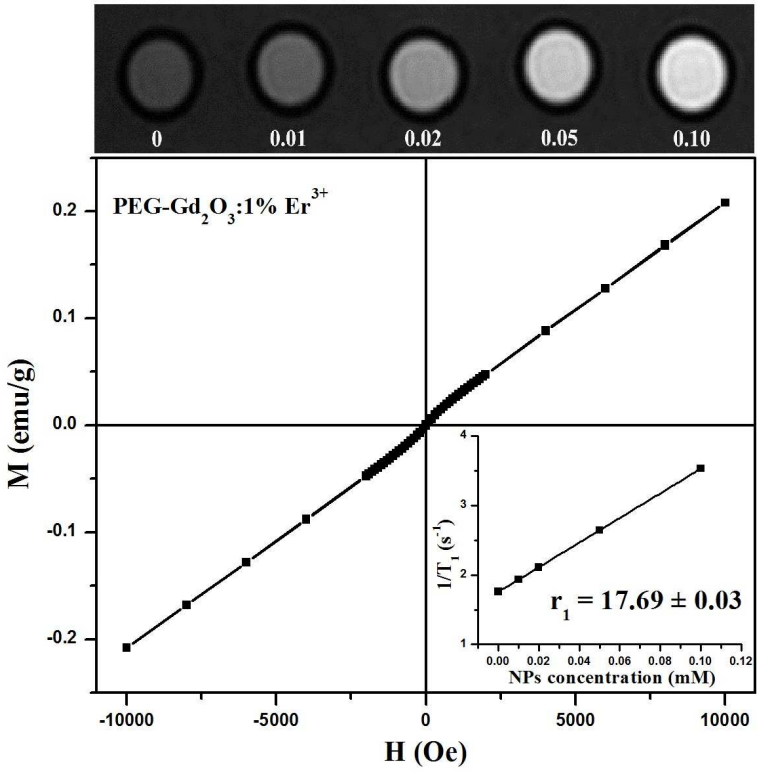

Fig.5 T_1-weighted images of various molar concentrations of PEG-coated Gd_2O_3:Er^{3+} NPs. QD-VSM measurements of PEG-coated Gd_2O_3:Er^{3+} NPs. Relaxation rate r_1 ($1/T_1$) versus various molar concentrations of PEG-coated Gd_2O_3:Er^{3+} NPs at room temperature (Inset).

3.4 Cytotoxicity profiles

To confirm the biocompatibility and biosafety of PEG-coated Gd_2O_3:1% Er^{3+} NPs synthesized for applications to non-invasive imaging, it is essential to measure their cytotoxicity. The cytotoxicity profiles of PEG-coated Gd_2O_3:1% Er^{3+} NPs in C2C12 myoblastic cells were determined using a CCK-8 assay, as shown in Figure 6(A). The WST-8 absorbance of the cells decreased with increasing concentration of NPs. Significant ($p < 0.05$) cytotoxicity was recorded from 62.5 ppm, which resulted in an approximately 36% decrease in cell viability compared to the unexposed controls. Furthermore, the PEG-coated Gd_2O_3:1% Er^{3+} NPs triggered approximately 80% loss of cell viability at the highest concentration (250 ppm). These dose-dependent responses of the C2C12 cells to the NPs were also evident from morphological observations (Figure 6(B)). The untreated control and lower concentrations ($\leq$ 31.3 ppm) of NPs caused slight changes in the cellular morphology. At higher concentrations ($\geq$ 62.5 ppm), however, the number of detached cells increased remarkably, indicating that the NPs might cause severe cellular deterioration, such as necrotic detachment and membrane degeneration. These dose-

RSC Advances Accepted Manuscript

dependent morphological alterations induced by NPs in C2C12 cells agreed well with their cytotoxicity profiles. The IC_{50} value of the PEG-coated Gd_2O_3:1% Er^{3+} NPs was calculated to be approximately 93 ppm. Considering the *in vitro* cytotoxicity only, the NPs synthesized in the present study may be applied safely for live-cell imaging and MRI at concentrations below 10 ppm.

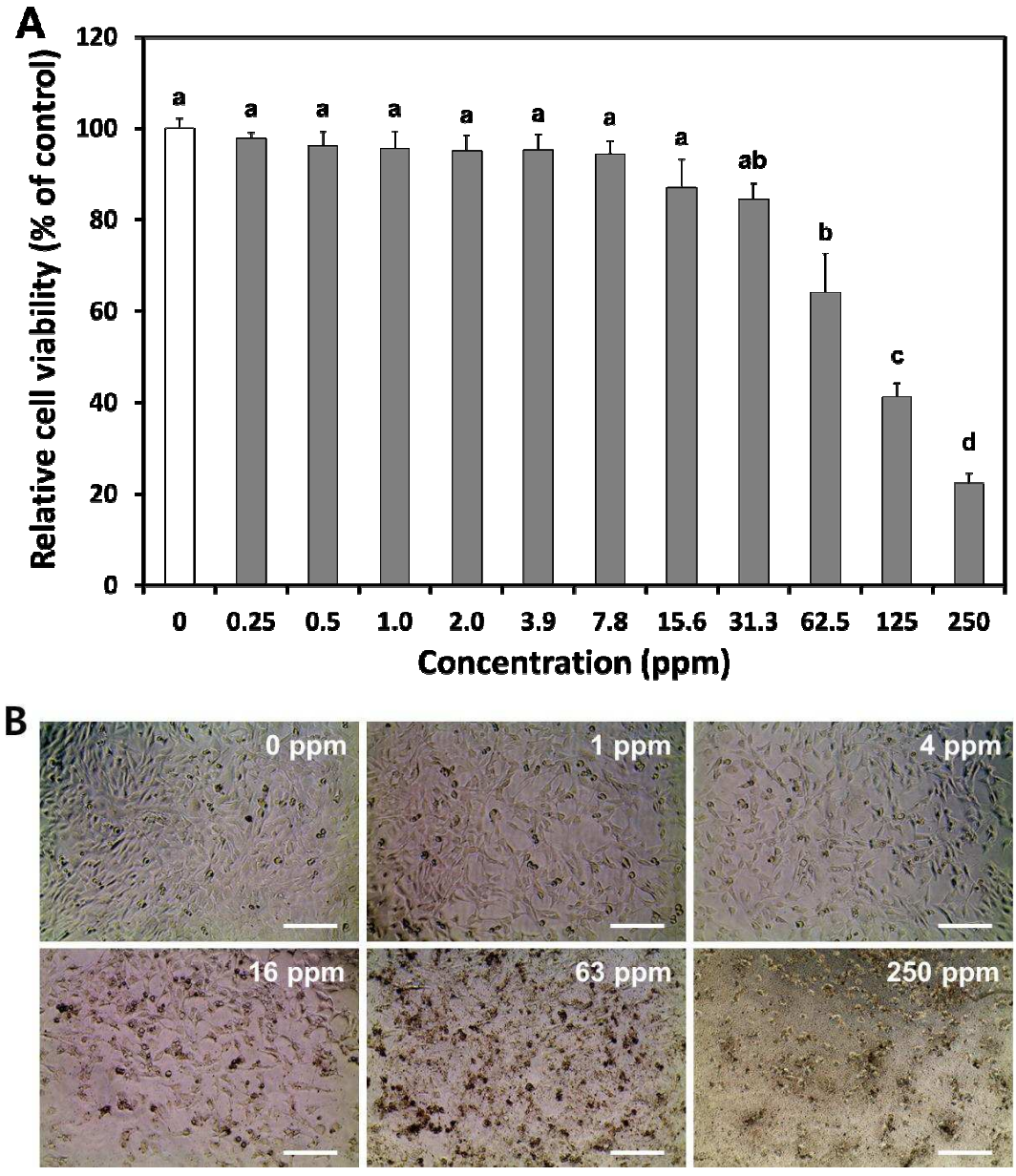

Fig. 6. Dose-dependent responses of C2C12 cells to PEG-coated Gd_2O_3:1% Er^{3+} NPs. (A) Cytotoxicity profiles of NPs. Relative cell viability of C2C12 cells exposed to increasing

RSC Advances Accepted Manuscript

concentrations (0 ~ 250 ppm) of NPs was evaluated using the CCK-8 assay. Data were expressed as mean ± standard deviation (SD) based on at least duplicate observations from three independent experiments. Different letters (a-safe, ab – relatively safe, b – moderate, c – toxic, d – extremely toxic) denote significant differences between the nontreated control and cells treated with each concentration of NPs, $P < 0.05$. (B) Morphological alterations of C2C12 cells. The scale bar is 200 μm. All photographs shown in this figure are representative of six independent experiments with similar results.

3.5 Cellular uptake and imaging

To examine the cellular uptake and cell imaging potentials of PEG-coated Gd_2O_3:1% Er^{3+} NPs, the cultured monolayer of C2C12 cells was incubated for 2 h in the culture medium with a NP suspension at a concentration of 10 ppm. Figure 7 shows fluorescence microscopy images of C2C12 cells after incubation with the NP suspension. After co-labeling with NPs and DAPI for cell nuclei counterstaining, the cells exhibited a similar morphology to that of normal muoblasts (Figure 7(A)). The bright green fluorescence from NP (Figure 7(B)) was observed mainly in the cytoplasm rather than inside the nuclei, suggesting that the NPs could make cell imaging possible through efficient internalization into the cells with a uniform distribution in the cytoplasm. The intensive blue fluorescence in Figure 7(C) indicates the nuclei counterstained by DAPI. In this figure, the fluorescence image (Fig. 7(D)) is the overlaying image of (B) and (C). Therefore, the PEG-coated Gd_2O_3:1% Er^{3+} NPs are promising as a sensitive T_1 contrast agent for clinical MRI applications compared to conventional Gd chelates, and have potential properties for luminescent cell tracking. MRI combined with molecular imaging will allow the monitoring of specific tissues or cell types, e.g., the detection of stem cell migration and cellular trafficking, differentiation, and transplant rejection. [18] Although the detailed mechanistic study for the cellular uptake of PEG-coated Gd_2O_3:1% Er^{3+} NPs was not examined, the NPs are believed to permeate into the cell membrane by non-specific endocytosis rather than by pinocytosis. [6, 19]

RSC Advances Accepted Manuscript

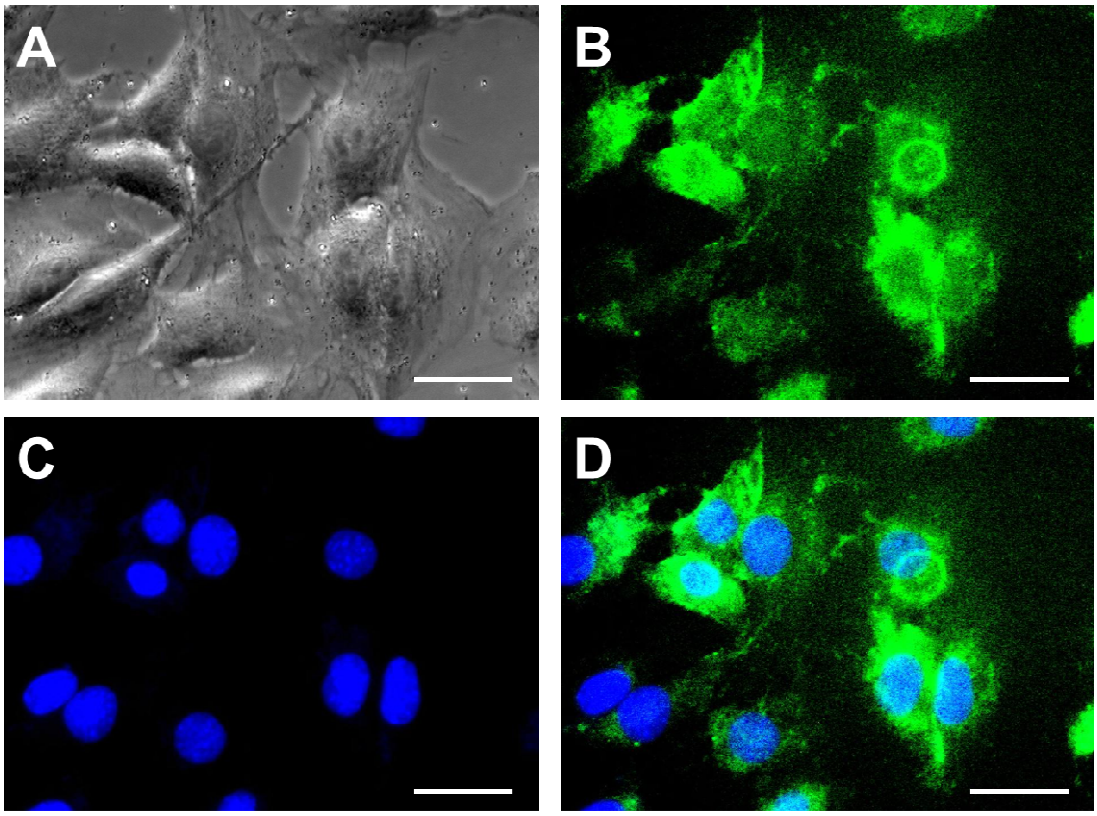

Fig. 7. Fluorescence micrographs (x 400) of C2C12 cells treated with 10 ppm PEG-coated Gd_2O_3:1% Er^{3+} NPs for 2 h, followed by cell nuclei counterstaining with 10 µmol/L DAPI. (A) Phase contrast image of the cells co-labelled with NPs and DAPI. (B) and (C) Fluorescence images of the cells collected at λ_{exc} = 980 nm (green from NPs) and λ_{exc} = 350 nm (blue, from DAPI), respectively. (D) Merged image of (B) and (C). The scale bar is 25 µm. All photographs shown in this figure are representative of six independent experiments with similar results.

Conclusion

In summary, uniform and well dispersed Gd_2O_3:1% Er^{3+} NPs were prepared using a urea homogeneous precipitation method. The morphology, structural, optical, and magnetic properties of the Gd_2O_3:1% Er^{3+} NPs were examined by FETEM, XRD, PL spectroscopy, and magnetic measurements, respectively. The surface modification of Gd_2O_3:1% Er^{3+} NPs using PEG molecules was investigated by FTIR spectroscopy. The UC luminescent properties of the Gd_2O_3:1% Er^{3+} NPs originate from the Er^{3+} dopant, which exhibits a strong emission peak at 562 nm. MRI relaxivity studies of the Gd_2O_3:1% Er^{3+} NPs showed high longitudinal relaxivity (r_1) of water protons, suggesting that Gd_2O_3:1% Er^{3+} NPs can be used as an efficient T_1 contrast agent. Therefore, the in vitro UC imaging of C2C12 cells and MRI relaxivity

RSC Advances Accepted Manuscript

measurements showed that the prepared PEG-capped Gd_2O_3:1% Er^{3+} NPs could serve as a dual-imaging agent for MRI/optical imaging.

Acknowledgments

This reseach was supported by the National Research Foundation of Korea (Grant No. 2012R1A1B3001357).

References

1. J. C. G. Bunzli, *Acc. Chem. Res.*, 2006, **39**, 53–61

2. T. Passuello, M. Pedroni, F. Piccinelli, S. Polizzi, P. Marzola, S. Tambalo, G. Conti, D. Benati, F. Vetrone, M. Bettinelli, A, Speghini , *Nanoscale*, 2012, **4**, 7682

3. F. C. J. M. van Veggel, C. Dong, N. J. J. Johnson and J. Pichaandi, *Nanoscale*, 2012, **4**, 7309

4. T. Grzyb, A. Gruszeczka, R. J. Wiglusz, Z. Sniadecki, B. Idzikowski, S. Lis, *J. Mater. Chem.*, 2012, **22**, 22989

5. J. Rao , A. Dragulescu-Andrasi , H. Yao , *Curr. Opin. Biotechnol.* 2007, **18**, 17

6. T. S. Atabaev, O. S. Jin, J. H. Lee, D. W. Han, H. H. T. Vu, Y. H. Hwang, H. K. Kim, *RSC Adv.*, 2012, **2**, 9495-9501

7. T. S. Atabaev, M. Kurisu, K. Konishi, N. H. Hong, *Americal Journal of Nanoscience and Nanotechnology* 2014, **2(1)**, 13-16

8. T. S. Atabaev, H. K. Kim, Y. H. Hwang, *Nanoscale Res. Lett.* 2013, **8**, 357

9. G. Jia, H. You, K. Liu, Y. Zheng, N. Guo, H. Zhang, *Langmuir* 2010, **26(7)**, 5122-5128

10. T.S. Atabaev, Z. Piao, Y. H. Hwang, H. K. Kim, H. H. Nguyen, *J. Alloys Compd.* 2013, **572**, 113-117

11. T. S. Atabaev, J. H. Lee, D.- W. Han, Y.H. Hwang, H.K. Kim, *J. Biomed. Mater. Res. A* 2012, **100A**, 2287-2294

12. J. V. Jokerst, T. Lobovkina, R. N. Zare, S. S. Gambhir, *Nanomedicine-UK* 2011, **6**, 715-728

13. A. Larsson, T. Ekblad, O. Andersson, B. Liedberg, *Biomacromolecules* 2007, **8**, 287-295

14. H. Guo, N. Dong, M. Yin, W. Zhang, L. Lou, S. Xia, *J. Phys. Chem. B* 2004, **108**, 19205-19209

15. S. Chandra, F. L. Deepak, J. B. Gruber, D. K. Sardar, *J. Phys. Chem. C* 2010*,* **114**, 874-880

16. M. Ajmal, T.S. Atabaev, *Opt. Mater.* 2013, **35**, 1288-1292

17. A. J. L. Villaraza, A. Bumb, M. W. Brechbiel, *Chem. Rev.* 2010, **110**, 2921

RSC Advances Accepted Manuscript

18. A. Hedlund, M Ahrén, H. Gustafsson, N. Abrikossova, M. Warntjes, J. I. Jönsson, K. Uvdal, M. Engström, *Int J Nanomedicine* 2011, **6**, 3233-3240

19. T. S. Atabaev, J. H. Lee, J. J. Lee, D.- W. Han, Y.H. Hwang, H.K. Kim, N.H. Hong, *Nanotechnology* 2013, **24**, 345603

RSC Advances Accepted Manuscript